Biomimetic Synthesis

DOI: 10.1002/anie.200802481

Monitoring Biomimetic Platinum Nanocluster Formation Using Mass Spectrometry and Cluster-Dependent H_2 Production**

Sebyung Kang, Janice Lucon, Zachary B. Varpness, Lars Liepold, Masaki Uchida, Debbie Willits, Mark Young, and Trevor Douglas**

Protein cages, such as ferritins, viruses, and heat shock proteins, have been used as size-constrained reaction vessels to spatially limit nanoparticle growth, to encapsulate preformed nanomaterials, or for covalent attachment of organic molecules.[1–7] Although protein cages have been widely used as powerful templates for nanomaterials syntheses, the processes of metal ion accumulation and core formation within a protein cage are still poorly understood. This is mainly due to the lack of appropriate analytical tools that detect multiple transient state species simultaneously with sufficient resolution and accuracy. While most spectroscopic techniques provide averaged information of populations in a mixture, mass spectrometry can simultaneously resolve individual molecular masses present in a mixture.[8,9] Therefore, it is possible to concurrently detect multiple populations distributed within an ensemble and monitor their changes individually instead of averaging all signals. With the invention of soft ionization methods, such as electrospray ionization (ESI)[10] and matrix assisted laser desorption ionization (MALDI),[11] it has become possible to measure the intact mass of noncovalently associated macromolecular complexes[12–14] and isolated colloids.[15–17] Mass measurement of giant noncovalent protein complexes have been extensively studied[18–21] and preservation of solution structures in the gas phase inside mass spectrometers has been well demonstrated.[12–14] We used this approach to monitor Pt^{2+} binding and Pt^0 nanocluster formation in a protein cage template.

Herein, we have genetically and chemically modified *Listeria innocua* Dps (LiDps) for the controlled synthesis of platinum nanoclusters, analyzed the Pt^0 nanocluster growth by noncovalent mass spectrometry, and verified the activity of these nanoclusters as hydrogen production catalysts. This is the first report to precisely follow the transition from metal binding through nucleation and nanocluster formation using mass spectrometry.

The Dps (DNA binding protein from starved cells) from the Gram-positive bacterium *Listeria innocua* prevents oxidative damage of DNA by accumulating iron atoms within its central cavity to produce an iron oxide core similar to that of ferritins.[22,23] The LiDps consists of twelve identical 18 kDa subunits that self-assemble into a hollow protein cage having tetrahedral 23 symmetry (Figure 1).[22] The LiDps is consequently smaller than ferritin with an outer diameter of 9 nm and an inner cavity diameter of 5 nm with 0.8 nm pores at the threefold axis where molecules can pass through to the interior (Figure 1).[22] The LiDps has been used for mineralizing metal oxides, such as iron and cobalt oxides, and cadmium sulfide.[24–26] Herein we have extended this approach to encapsulate Pt^0 nanoparticles using the LiDps cage. We genetically modified the LiDps to enable site selective chemical modification to the interior of the LiDps cage by substitution of serine at position 138, located in the middle of helix E, with cysteine (S138C; Figure 1). We synthesized 5-iodoacetamido-1,10-phenanthroline (iodo-phen)[27] and labeled the introduced cysteines of the S138C mutant with no alteration of the protein cage architecture (see Figure F1 in the Supporting Information). Covalent attachment of metal binding ligands to the interior surface of the LiDps was expected to induce binding of Pt^{2+} ions and facilitate nucleation of Pt^{2+} ions.

The extent of reaction between the iodo-phen and LiDps cysteine thiols to form the corresponding thioether with loss

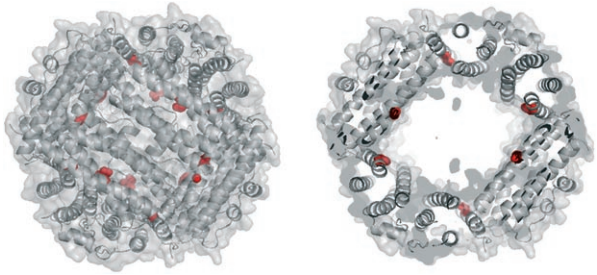

Figure 1. Surface and ribbon diagram representations of LiDps (PDB 1QGH) looking down the twofold symmetry axis (left) and a clipped view showing the interior space of the cage (right). Serine 138 residues substituted with cysteines, in the S138C mutant, are indicated in red.

[*] Dr. S. Kang, J. Lucon, Dr. Z. B. Varpness,[+] L. Liepold, Dr. M. Uchida, Prof. T. Douglas
Department of Chemistry and Biochemistry
Center for BioInspired Nanomaterials
Montana State University, Bozeman, Montana, 59717 (USA)
Fax: (+1) 406-994-5947
E-mail: myoung@montana.edu
D. Willits, Prof. M. Young
Department of Plant Science, Center for BioInspired Nanomaterials
Montana State University, Bozeman, Montana, 59717 (USA)
Fax: (+1) 406-994-5117
E-mail: tdouglas@chemistry.montana.edu
[+] Current address: Department of Physical and Life Science
Chadron State College, Chardron, NE 69337 (USA)

[**] We thank Susan Brumfield for assistance in TEM. This research was supported in part by grants from the National Science Foundation (CBET-0709358), Office of Naval Research (N00014-03-1-0692), the Department of Energy (DE-FG02-07ER46477), and Human Frontiers of Science Program (RGP61/2007).

Supporting information for this article is available on the WWW under http://dx.doi.org/10.1002/anie.200802481.

of I^- (Supporting Information, F2) was evaluated by measuring the molecular masses of subunits using electrospray ionization time-of-flight mass spectrometry (ESI-TOF MS) using previously described methods.[28,29] Attachment of the phenanthroline moiety to the LiDps subunit resulted in a 236 unit mass increase (Supporting Information, F2). Two major populations were detected from the iodo-phen treated S138C LiDps. Component analysis of the charge state distributions revealed that the dominant species in the iodo-phen treated S138C LiDps sample were a 18301.4 Da subunit (85%) and a 18065.4 Da subunit (15%). These observed masses are in excellent agreement with the values predicted for a LiDps protein subunit modified with a single phenanthroline moiety (18300.7 Da) and the unmodified subunit (18064.7 Da; Figure 2A). Wild-type (wt) LiDps, which does not have an intrinsic cysteine, was treated in parallel as a control and no modification was observed under identical reaction conditions (Supporting Information, F3).

We confirmed the dodecameric cage architecture of the LiDps by measuring the intact cage masses of the S138C and iodo-phen treated S138C LiDps (phen-S138C LiDps; Figure 2B). The typical charge state distribution of dodecameric LiDps was observed with unmodified S138C LiDps (Figure 2B, bottom panel). The charge state distribution of the phen-S138C LiDps cage was shifted to higher m/z and its mass increase was 2375 Da, which corresponds to addition of 10.1 phenanthroline moieties (236 Da) per cage on average (Figure 2B, top panel and inset values). The mass increase for the intact phen-S138C LiDps agreed well with the extent of modification determined by subunit mass analysis (Figure 2).

For monitoring Pt^{2+} ion binding, phen-S138C LiDps was treated with various amounts of Pt^{2+} ions (0, 12, 24, 48, 100, and 200 Pt^{2+} per cage) and equilibrated at 4°C overnight. Unbound Pt^{2+} ions were removed by size exclusion chromatography (SEC) and the Pt^{2+}-phen-S138C Dps complexes were analyzed by noncovalent mass spectrometry. Wt and unlabeled S138C LiDps were also treated in parallel to investigate the direct role of the phenanthroline moiety in Pt^{2+} ion binding. While phen-S138C LiDps contained 43 Pt^{2+} ions with a theoretical loading of 200 Pt^{2+} per cage (Figure 3), unmodified S138C and wt LiDps contained 23 and 16 Pt^{2+} ions, respectively, at equivalent Pt^{2+} ion loading (Supporting Information, F4) suggesting that the phenanthroline moiety facilitates additional Pt^{2+} binding.

In order to follow Pt^0 nanocluster formation, phen-S138C LiDps was incubated with the same range of Pt^{2+} ion loadings (0, 12, 24, 48, 100, and 200 Pt^{2+} per cage) at 4°C overnight and subsequently photoreduced. Analysis of the reaction product by SEC revealed that the Pt^0 mineralized phen-S138C LiDps eluted at the same position as the untreated control phen-S138C LiDps. This unaltered elution profile indicates that the Pt^{2+} binding and Pt^0 mineralization occur selectively within

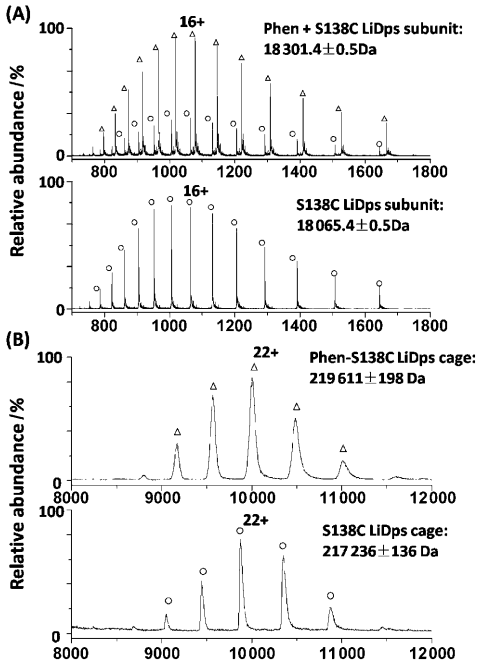

Figure 2. Mass spectrometric analyses of the subunit and intact LiDps before and after treatment with 5-iodoacetamido-1,10-phenanthroline; charge state distributions for modified (△) and unmodified S138C LiDps cages (○) are shown. A) Mass spectra of subunits. Charged peaks (16+) of subunit either unmodified or modified with a single phenanthroline moiety are indicated. B) Noncovalent mass spectra of intact LiDps cages with charged peaks (22+) of iodo-phen treated and untreated cages indicated.

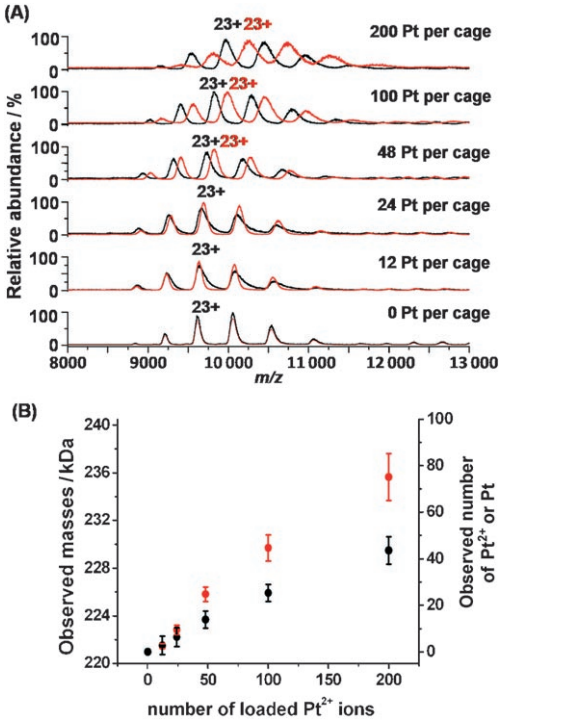

Figure 3. A) Overlaid mass spectra of the Pt^{2+} ion bound (black) and Pt^0 mineralized (red) phen-S138C LiDps cages at various loading ratios of Pt^{2+} (0, 12, 24, 48, 100, and 200 Pt^{2+} ions per cage, bottom to top). Charged peaks (23+) of the cages are indicated. B) Plots of the observed masses (left y axis) and converted numbers (right y axis) of Pt^{2+} ion bound (black circles) and Pt^0 mineralized (red circles) phen-S138C LiDps cages according to the initial Pt^{2+} ion loadings. Deviations of Pt^{2+}-ion or Pt^0-atom contents in the broadened peaks were determined by calculating the half width at the half height of each peak and comparing to a 0 loading control.

the inner cavity of the cages and does not alter the cage architecture (Supporting Information, F5). However, uncontrolled particle growth was observed through a shift in the SEC profile with wt and unlabeled S138C LiDps cages under identical reaction condition (Supporting Information, F6). Charge state distributions of both Pt^{2+} ion bound (black) and Pt^0 nanoclustered phen-S138C LiDps (red) were shifted to higher m/z compared to the untreated phen-S138C LiDps in accordance with the increasing numbers of Pt^{2+} loaded (Figure 3A). Only one population was observed at each Pt^{2+} loading (Figure 3A) implying that binding or nanocluster formation events occur homogeneously throughout the cage population rather than in an all-or-nothing manner. However, peak broadening at the high Pt^{2+} loadings was observed (Figure 3A) indicating that individual phen-S138C LiDps contains slightly different amounts of Pt^{2+} or Pt^0 within a narrow distribution with a maximum deviation of 10 Pt^0 at loading of 200 Pt^{2+} per cage as shown in Figure 3B. Charge state distributions of Pt^0 nanoclustered phen-S138C LiDps were shifted to higher m/z compared to that of Pt^{2+} ion bound phen-S138C LiDps suggesting increased Pt^{2+} incorporation upon photoreduction (Figure 3A). Based on the mass cacu-lations, 2.8, 6.3, 13.9, 25.3, and 43.5 Pt^{2+} ions were bound to phen-S138C LiDps with theoretical Pt^{2+} ion loadings of 12, 24, 48, 100, and 200 Pt^{2+} ions per cage, respectively, whereas Pt^0 nanoclusters containing 2.4, 9.4, 24.8, 44.6, and 75 Pt^0 atoms were formed in phen-S138C LiDps with the same range of Pt^{2+} ion loadings (Figure 3B). Taken together these results suggest that the introduced Pt^{2+} ions first enter the cages and bind to the covalently attached phenanthroline moiety and that free Pt^{2+} ions inside are recruited by the pre-bound Pt^{2+} ions upon photoreduction to form the Pt^0 nanoclusters.

To verify core formation, we attempted to observe the Pt^0 nanoclusters inside the cages using transmission electron microscopy (TEM), but we could not detect Pt^0 cores inside phen-S138C LiDps (Supporting Information, F7). However, a core size of 75 Pt^0 is estimated to have an approximately 1 nm diameter which is at the detection limit of the instrument. Therefore, we may not have detected distinct cores because of technical limitations rather than the lack of core formation.

Pt^0 nanoparticles are known to be excellent catalysts for proton reduction and hydrogen production.[30,31] It has been suggested that their catalytic activity is dependent upon the Pt^0 particle size.[32] We have previously demonstrated efficient hydrogen production using the Pt^0 mineralized heat shock protein cages in conjunction with a photochemical system.[6] To move toward a more simple assay, we have implemented a photosystem based on $[Ir(ppy)_2(bpy)]^+$ (ppy = 2-phenylpyridine; bpy = 2,2′-bipyridine) which has been shown to act as a mediatorless photocatalyst for hydrogen production in conjunction with Pt^0 colloid.[33] We used the Ir based photocatalyst as a tool to investigate the loading required to create catalytic Pt^0 clusters for hydrogen production (Figure 4 and Supporting Information, F8). The Ir complex only control corroborated previous reports that the complex can produce small amounts of hydrogen without a Pt catalyst present.[33] While the phen-S138C LiDps samples with equal to or less than 45 Pt^0 (theoretical loading of 100 Pt^{2+} per cage) produced hydrogen near baseline levels, the 75 Pt^0 (theoretical loading of 200 Pt^{2+} per cage) containing phen-S138C LiDps generated approximately four times more hydrogen than the background level (Figure 4B and Supporting Information, F8). These data support the idea that the 75 Pt atoms may form a sufficiently large nanocluster rather than multiple nanoclusters in the phen-S138C LiDps. In contrast, the 45 Pt^0, or lower Pt^0, containing cages appear to have failed to form a sufficiently large cluster to catalyze hydrogen production.

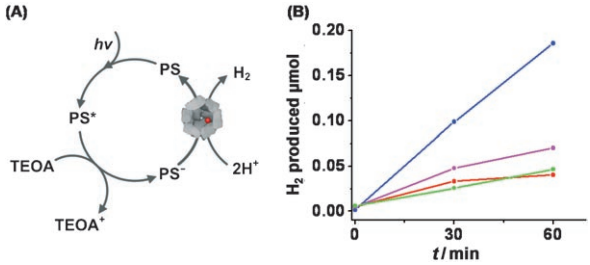

Figure 4. Hydrogen production from the Pt^0 mineralized phen-S138C LiDps. A) Schematic representation of the light-mediated hydrogen production from Pt^0 nanoclustered phen-S138C LiDps. The photosensitizer (PS) employed in this process is $[Ir(ppy)_2(bpy)]^+$. B) Time-dependent hydrogen production of Ir complex only (red), 25 Pt^0 atoms (green), 44 Pt^0 atoms (magenta), and 75 Pt^0 atoms (blue) mineralized phen-S138C LiDps.

In conclusion, we have successfully resolved Pt^{2+} ion binding and Pt^0 nanocluster formation inside the protein cages at near atomic resolution using mass spectrometry. In addition, we have demonstrated catalytic Pt^0 nanocluster formation for hydrogen production within the Dps cage. This high resolution analysis has been made possible by using the genetically engineered and chemically functionalized LiDps for directed nanocluster growth. Better understanding of biomimetic mineralization processes may give us greater insight into controlled material synthesis under mild conditions. In particular, thoroughly elucidating the relationship between Pt^0 nanocluster sizes and the total quantity of hydrogen produced may lead to the development of more efficient hydrogen production systems.

Experimental Section

Mutagenesis, protein expression, and purification: Cysteine substitution of serine 138 was generated by Quick change PCR protocol using pET-30b based plasmids encoding genes for LiDps. The amplified DNAs were transformed into competent *E.coli* strain BL21 (DE) and S138C LiDps was over-expressed in *E. coli* and purified as previously described.[24]

Phen modification of the S138C LiDps and purification: Synthesis of 5-iodoacetamido-1,10-phenanthroline (iodo-phen) was carried out as previously described.[27] The final product was confirmed by mass spectrometry. The S138C LiDps was incubated with 3 molar equivalents of iodo-phen at 4 °C overnight. Reactions were loaded onto a 10 × 300 mm Superose 6 (Amersham Bioscience) size exclusion column and eluted with buffer containing 50 mM 4-morpholineethanesulfonic acid (MES), 100 mM NaCl (pH 6.5) at a rate of 0.5 mL min^{-1}.

Mass spectrometry: Subunit masses of the iodo-phen treated and untreated S138C LiDps cages were analyzed by ESI-Q-TOF mass spectrometry (Q-TOF Premier, Waters) interfaced to a Waters UPLC and autosampler. Samples were loaded onto the BioBasic SEC-300

column (5 μm, 250 L × 1.0 mm I.D, Thermo Scientific) and eluted with the buffer containing 40 % isopropyl alcohol, 59.9 % water, and 0.1 % formic acid isocratically with a rate of 25 μL min^{-1}. Mass spectra were acquired in the range of *m*/*z* 50–5000 and processed using component analysis from MassLynx version 4.1 to obtain average masses from multiple charge state distributions. Mass analyses of the intact LiDps cages were carried out on samples in 10 mM triethylammonium acetate buffer (pH 6.8).[34] Spectra were acquired in the range of *m*/*z* 50–30 000 by directly infusing samples into the mass spectrometer at a flow rate of 20 μL min^{-1}. Source and desolvation temperatures were 80 °C and 120 °C, respectively. Collisional focusing, which facilitated the focusing and transmission of ionized LiDps cages in vacuo, was achieved by increasing the source pressure to approximately 7.0 mbar.[35] The capillary voltage and the sample cone voltage were 3000 and 50 V, respectively. Pressure in the collision cell and the TOF tube were maintained at 1.0×10^{-2} and 2.0×10^{-6} mbar, respectively. Mass calibration was accomplished by directly infusing aqueous CsI (50 mg mL^{-1}) at 0.5 μL min^{-1}. Charge states and masses were obtained from the spectral data using MassLynx version 4.1 software (Waters). All assigned masses were manually verified. Deviations of the Pt^{2+} ion and Pt^0 contents in the broadened peaks were determined by calculating the half-width at the half-height of each peak and comparing with a 0 loading control.

Pt^{2+} ion binding and Pt^0 nanocluster formation: phen-S138C LiDps (200 μL at 1 mg mL^{-1} in 50 mM MES, 100 mM NaCl, pH 6.5) was mixed with the appropriate amount of 2 mM K_2PtCl_4 for a theoretical loading of either 0, 12, 24, 48, 100, or 200 Pt^{2+} per cage. To each sample 25 mM MES (pH 6.5) was added for a final volume of 400 μL. After incubating at 4 °C overnight, a four-fold excess of 4 mM sodium citrate was added to each cuvette and then they were immediately illuminated with a 150 W Xe arc lamp (175 W, Lambdz-LS, Sutter Instruments) equipped with an IR filter (10 cm water filter) and a UV cutoff filter (UV absorbing glass) for 45 min. The light flux was measured using an Extech Instrument EasyView light meter. The sample temperature was maintained at 40 °C with a water bath.[36,37] After mineralization each sample was loaded onto a 10 × 300 mm Superose 6 (Amersham Bioscience) size exclusion column and eluted with 50 mM MES, 100 mM NaCl (pH 6.5) at a rate of 0.5 mL min^{-1}.

Light induced hydrogen production: The remaining 0, 48, 100, and 200 Pt^{2+} ion per cage samples (approximately 0.62 nM) were mixed with 53.5 μL of 33 mM $[Ir(ppy)_2(bpy)]PF_6$ and 2000 μL of a acetonitrile/water/triethanolamine (TEOA) mixture (9:3:1).[33] The photosensitizer only control was mixed in the same manner adding 53.5 μL extra 9:3:1 acetonitrile/water/TEOA to make the same final volume. Samples were septum sealed and degassed under N_2 and vacuum alternatively three times. Each sample was illuminated for 1 h at 25 °C with the same lamp used for photoreduction. Headspace samples were analyzed on a Shimadzu GC-8A TCD with a 1.83 m × 0.32 cm 80/100 Porapak Supelco column using argon as carrier gas.[6] Bulk H_2 gas was used as a standard to quantify the sample H_2 production.

Received: May 27, 2008
Revised: July 8, 2008
Published online: September 3, 2008

Keywords: H_2 production · mass spectrometry · nanoclusters · platinum · protein cages

[1] T. Douglas, M. Young, *Nature* **1998**, *393*, 152 – 155.
[2] M. T. Klem, D. Willits, D. J. Solis, A. M. Belcher, M. Young, T. Douglas, *Adv. Funct. Mater.* **2005**, *15*, 1489 – 1494.
[3] M. Knez, A. Bittner, F. Boes, C. Wege, H. Jeske, E. Mai, K. Kern, *Nano Lett.* **2003**, *3*, 1079 – 1082.
[4] S. Mann, G. A. Ozin, *Nature* **1996**, *382*, 313 – 318.
[5] M. Uchida, M. T. Klem, M. Allen, P. Suci, M. Flenniken, E. Gillitzer, Z. Varpness, L. O. Liepold, M. Young, T. Douglas, *Adv. Mater.* **2007**, *19*, 1025 – 1042.
[6] Z. Varpness, J. W. Peters, M. Young, T. Douglas, *Nano Lett.* **2005**, *5*, 2306 – 2309.
[7] M. L. Flenniken, D. A. Willits, S. Brumfield, M. J. Young, T. Douglas, *Nano Lett.* **2003**, *3*, 1573 – 1576.
[8] A. Poliakov, E. van Duijn, G. Lander, C. Y. Fu, J. E. Johnson, P. E. Prevelige, A. J. R. Heck, *J. Struct. Biol.* **2007**, *157*, 371 – 383.
[9] F. Sobott, J. L. Benesch, E. Vierling, C. V. Robinson, *J. Biol. Chem.* **2002**, *277*, 38921 – 38929.
[10] J. B. Fenn, M. Mann, C. K. Meng, S. F. Wong, C. M. Whitehouse, *Science* **1989**, *246*, 64 – 71.
[11] K. Tanaka, H. Waki, Y. Ido, S. Akita, Y. Yoshida, T. Yoshida, T. Matsuo, *Rapid Commun. Mass Spectrom.* **1988**, *2*, 151 – 153.
[12] J. L. Benesch, C. V. Robinson, *Curr. Opin. Struct. Biol.* **2006**, *16*, 245 – 251.
[13] B. Bothner, G. Siuzdak, *ChemBioChem* **2004**, *5*, 258 – 260.
[14] A. J. R. Heck, R. H. H. van den Heuvel, *Mass Spectrom. Rev.* **2004**, *23*, 368 – 389.
[15] A. Dass, A. Stevenson, G. R. Dubay, J. B. Tracyt, R. W. Murray, *J. Am. Chem. Soc.* **2008**, *130*, 5940 – 5946.
[16] J. B. Tracy, G. Kalyuzhny, M. C. Crowe, R. Balasubramanian, J. P. Choi, R. W. Murray, *J. Am. Chem. Soc.* **2007**, *129*, 6706 – 6707.
[17] N. K. Chaki, Y. Negishi, H. Tsunoyama, Y. Shichibu, T. Tsukuda, *J. Am. Chem. Soc.* **2008**, *130*, 8608 – 8610.
[18] N. Kitagawa, H. Mazon, A. J. R. Heck, S. Wilkens, *J. Biol. Chem.* **2007**, *283*, 3329 – 3337.
[19] O. Esteban, R. A. Bernal, M. Donohoe, H. Videler, M. Sharon, C. V. Robinson, D. Stock, *J. Biol. Chem.* **2007**, *283*, 2595 – 2603.
[20] M. Fandrich, M. A. Tito, M. R. Leroux, A. A. Rostom, F. U. Hartl, C. M. Dobson, C. V. Robinson, *Proc. Natl. Acad. Sci. USA* **2000**, *97*, 14151 – 14155.
[21] A. M. Last, C. V. Robinson, *Curr. Opin. Chem. Biol.* **1999**, *3*, 564 – 570.
[22] A. Ilari, S. Stefanini, E. Chiancone, D. Tsernoglou, *Nat. Struct. Biol.* **2000**, *7*, 38 – 43.
[23] S. Stefanini, S. Cavallo, B. Montagnini, E. Chiancone, *Biochem. J.* **1999**, *338*, 71 – 75.
[24] M. Allen, D. Willits, J. Mosolf, M. Young, T. Douglas, *Adv. Mater.* **2002**, *14*, 1562 – 1565.
[25] M. Allen, D. Willits, M. Young, T. Douglas, *Inorg. Chem.* **2003**, *42*, 6300 – 6305.
[26] K. Iwahori, T. Enomoto, H. Furusho, A. Miura, K. Nishio, Y. Mishima, I. Yamashita, *Chem. Mater.* **2007**, *19*, 3105 – 3111.
[27] C. H. B. Chen, D. S. Sigman, *Proc. Natl. Acad. Sci. USA* **1986**, *83*, 7147 – 7151.
[28] S. Kang, A. M. Hawkridge, K. L. Johnson, D. C. Muddiman, P. E. Prevelige, *J. Proteome Res.* **2006**, *5*, 370 – 377.
[29] S. Kang, G. C. Lander, J. E. Johnson, P. E. Prevelige, *ChemBioChem* **2008**, *9*, 514 – 518.
[30] M. J. Esswein, D. G. Nocera, *Chem. Rev.* **2007**, *107*, 4022 – 4047.
[31] M. Graetzel, *Acc. Chem. Res.* **1981**, *14*, 376 – 384.
[32] E. Greenbaum, *J. Phys. Chem.* **1988**, *92*, 4571 – 4574.
[33] L. L. Tinker, N. D. McDaniel, P. N. Curtin, C. K. Smith, M. J. Ireland, S. Bernhard, *Chem. Eur. J.* **2007**, *13*, 8726 – 8732.
[34] D. Lemaire, G. Marie, L. Serani, O. Laprevote, *Anal. Chem.* **2001**, *73*, 1699 – 1706.
[35] N. Tahallah, M. Pinske, C. S. Maier, A. J. R. Heck, *Rapid Commun. Mass Spectrom.* **2001**, *15*, 596 – 601.
[36] R. M. Wilenzick, D. C. Russell, R. H. Morriss, S. W. Marshall, *J. Chem. Phys.* **1967**, *47*, 533 – 536.
[37] M. T. Klem, J. Mosolf, M. Young, T. Douglas, *Inorg. Chem.* **2008**, *47*, 2237 – 2239.

